

The Performance of a Horizontal Flexible Membrane Breakwater in Waves

by

I.H. Cho⁽¹⁾, S.W. Hong⁽¹⁾ and M.H. Kim⁽²⁾

파랑중 수평형 유연막 방파제 성능해석

조일형⁽¹⁾, 홍석원⁽¹⁾, 김무현⁽²⁾

Abstract

The interaction of monochromatic incident waves with a horizontal flexible membrane is investigated in the context of two-dimensional linear hydro-elastic theory. First, analytic diffraction and radiation solutions for a submerged impermeable horizontal membrane are obtained. Second, the theoretical prediction was compared with a series of experiments conducted in a two-dimensional wave tank at Texas A&M University. The measured reflection and transmission coefficients reasonably follow the trend of predicted values. Using the developed computer program, the performance of surface-mounted or submerged horizontal membrane wave barriers is tested with various system parameters and wave characteristics. It is found that the properly designed horizontal flexible membrane can be an effective wave barrier.

요약

본 연구에서는 수면 밑 일정한 깊이에 잠긴 유연한 천이 파도중 수평으로 놓여 있을 때 유연막과 파도의 상호작용 문제를 살펴보았다. 파도와 유연막의 상호작용을 고려하기 위하여 선형 유탄성 이론을 사용하였다. 계산 예로 유연막의 형태, 잠긴 깊이 그리고 유연막에 걸리는 초기 장력을 변화시키면서 반사율과 투과율 그리고 유연막의 변형을 살펴보았다. 또한 Texas A&M 대학의 2차원 수조에서 모형실험을 수행하여 실험결과와 해석해를 비교하였다. 실험결과와 해석결과는 정성적으로 잘 일치하고 있음을 확인하였다. 개발된 설계 프로그램을 이용하여 설치 해역의 파랑 특성에 적합한 최적의 유연막 방파제를 설계, 제작할 수 있으리라 사료된다.

Keywords: 유연막(flexible membrane), 방파제(breakwater), 반사율(reflection coefficient), 투과율(transmission coefficient), 모형실험(model test), 선형포텐셜 이론(linear potential theory), 고유함수전개법(eigen-function expansion method)

(1) Members, Korea Research Institute of Ships and Ocean Engineering

(2) Associate Prof., Dept. of Civil Engineering, Texas A & M University

1. Introduction

Most floating wave barriers are known to be ineffective in long waves unless its size is comparable to the pertinent wave length. Therefore, to be a very effective wave barrier, the structural dimension has to be large and the resulting high construction cost has been a major obstruction for the realization of many floating-breakwater projects. During the past decade, there has been a gradual increase of interest in the use of flexible plate or membrane as an effective, inexpensive wave barrier. In particular, the membrane is light and rapidly deployable, and thus it may be an ideal candidate as a portable temporary breakwater.

There have been many theoretical and experimental studies with regard to the performance of vertical flexible wave barriers. For example, the efficiency of a vertical-elastic-plate breakwater clamped at the seafloor was investigated by Lee & Chen [1990] and Williams et al. [1991]. Abul Azm [1994] also showed that the efficiency of the elastic beam breakwater can be improved by tuning two vertical screens. On the other hand, the performance of a vertical-screen membrane breakwater, which is equivalent to the tensioned elastic-beam breakwater with zero bending rigidity, was investigated by Thomson et al. [1992], Aoki et al. [1994], Kim & Kee [1996], Kee & Kim [1997], and Williams [1996]. Using the linear wave theory and membrane-motion equation, Kim & Kee [1996] and Kee & Kim [1997] showed that almost complete reflection was possible by a vertically flexible membrane despite appreciable sinusoidal motions, which tend to generate only exponentially decaying local (evanescent) waves in the lee side. The theory was compared favorably with 2-D tank

experiments [Kim et al., 1996]. This interesting phenomenon can also be confirmed by the classical wavemaker theory [Dean & Dalrymple, 1984].

One of the major problems associated with the use of flexible vertical screen is the expected large wave loading and possible blockage of currents. In view of this, the possibility of using alternative horizontal membrane is investigated in this paper. In particular, the submerged horizontal membrane does not hamper the seascape and also allows the passage of ships and currents. Since the horizontal membrane does not directly block incoming waves, the diffracted and radiated waves including various elastic modes have to be properly tuned to be an effective wave barrier. The formulation of the interaction of a submerged horizontal membrane with waves is in general more complicated than the vertical-membrane case. Siew & Hurley[1977] and McIver[1985], for instance, studied the diffraction of linear waves by a submerged rigid flat plate. They showed that it can reflect significant amount of incident wave energy in a certain wave-frequency region. In this paper, it is shown that the overall wave-blocking efficiency can be greatly improved by using horizontal flexible membrane instead of rigid plate. The relevant hydro-elastic theory is formulated in Sec.2.

Finally, in Sec.4, the performance of various designs of horizontal-membrane wave barriers is studied for a variety of wave conditions or water depths. It is shown that the system can be highly efficient if properly designed and the high performance region can be controlled by changing relevant design parameters. The results are summarized and concluding remarks are given in Sec.5.

2. Mathematical Formulation and Analytic Solutions

We consider the interaction of a horizontal membrane wave barrier with monochromatic incident waves. Cartesian axes are chosen with the x-axis along the mean free surface and y-axis pointing vertically upwards. The water depth is denoted by h and the submergence depth of the membrane by d . It is assumed that both ends of the membrane are fixed at $x = \pm a$, and a uniform tension T is applied on the membrane in the x direction (see Fig.1a).

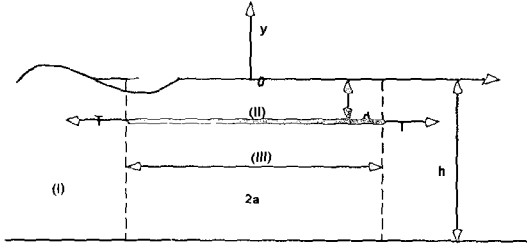


Fig. 1a Definition sketch for horizontal Impermeable flexible membrane

It is also assumed that the fluid is incompressible and inviscid, and the wave and membrane motions are small so that linear potential theory can be used. The fluid particle velocity can then be described by the gradient of a velocity potential $\Phi(x, y, t)$. Assuming harmonic motion of frequency ω , the velocity potential can be written as $\Phi(x, y, t) = \Re[\phi(x, y)e^{-i\omega t}]$. Similarly, the vertical displacement of membrane can be written as

$$\zeta(x, t) = \Re[\xi(x)e^{-i\omega t}], \quad (1)$$

where $\xi(x)$ is the complex displacement of membrane.

The velocity potential ϕ satisfies the

Laplace equation

$$\frac{\partial^2 \phi}{\partial x^2} + \frac{\partial^2 \phi}{\partial y^2} = 0 \text{ in the fluid,} \quad (2)$$

with the following boundary conditions

$$\frac{\partial \phi}{\partial y} - v\phi = 0 \text{ on } y = 0. \quad (v = \frac{\omega^2}{g}) \quad (3)$$

$$\frac{\partial \phi}{\partial y} = 0 \text{ on } y = -h. \quad (4)$$

$$\lim_{|x| \rightarrow \infty} \left(\frac{\partial \phi}{\partial x} \pm ik_1 \phi \right) = 0. \quad (5)$$

$$\frac{\partial \phi}{\partial y} = -i\omega \xi \text{ on } y = -d, -a \leq x \leq a. \quad (6)$$

The complex displacement of membrane can be expanded in terms of a set of natural modes of the membrane:

$$\xi(x) = \sum_{l=1}^{\infty} \varsigma_l f_l(x), \quad (7)$$

where ς_l is the unknown complex modal amplitude corresponding to the l th mode. The modal functions and eigenvalues of the membrane satisfying the membrane equation and the end condition are given by

$$f_l(x) = \begin{cases} f_l^S(x) = \cos \frac{\lambda_l^S x}{a}, & \lambda_l^S = \frac{[2(l-1)+1]\pi}{2}, \\ f_l^A(x) = \sin \frac{\lambda_l^A x}{a}, & \lambda_l^A = l\pi \quad (l = 1, 2, 3, \dots), \end{cases} \quad (8)$$

where the superscripts S and A denote symmetric and asymmetric modes about $x = 0$, respectively. The modal functions given in equation (8) are orthogonal to each other in the interval $[-a, a]$:

$$\int_{-a}^a f_i(x) f_j(x) dx = \begin{cases} a & i = j \\ 0 & i \neq j. \end{cases} \quad (9)$$

Including all the flexible membrane modes, the complex potential $\phi(x, y)$ can be expressed in the form

$$\begin{aligned}\phi(x, y) &= \phi_D(x, y) + \sum_{l=1}^{\infty} g_l \phi_{Rl}(x, y), \\ \phi_D(x, y) &= \phi_I(x, y) + \phi_S(x, y),\end{aligned}\quad (10)$$

where ϕ_D is the diffraction potential and ϕ_S, ϕ_{Rl} denote the scattering and radiation potential, respectively. The incident wave potential ϕ with unit amplitude is given by

$$\phi_I(x, y) = -\frac{ig \cosh k_1(y+h)}{\omega \cosh k_1 h} e^{k_1 x}, \quad (11)$$

where g is the gravitational acceleration, and k_1 is the wave number satisfying the usual dispersion relation

$$\frac{\omega^2}{g} = k_1 \tanh k_1 h. \quad (12)$$

2.1 Diffraction Problem

The diffraction potential ϕ_D satisfies equation (2)-(5) and the following membrane boundary condition:

$$\frac{\partial \phi_D}{\partial y} = 0 \text{ on } y = -d, -a \leq x \leq a. \quad (13)$$

In ϕ_D into symmetric and asymmetric parts. the following, the symmetry of the fluid and membrane is used by splitting

$$\phi_D(x, y) = \phi_D^S(x, y) + \phi_D^A(x, y), \quad (14)$$

where

$$\begin{aligned}\phi_D^S(-x, y) &= \phi_D^S(x, y), \quad \frac{\partial \phi_D^S}{\partial x} = 0 \text{ on } x = 0, \\ \phi_D^A(-x, y) &= -\phi_D^A(x, y), \quad \phi_D^A = 0 \text{ on } x = 0.\end{aligned}$$

The fluid domain is divided into three regions, as shown in Fig.1a. Region (I) is defined by $x \leq -a, -h < y < 0$, region (II) by $|x| \leq a, -d < y < 0$ and region (III) by $|x| \leq a, -h < y < -d$.

The symmetric diffraction potentials in the

three fluid regions are written as

$$\begin{aligned}\phi_D^{S(1)} &= -\frac{ig}{\omega} \left\{ \frac{1}{2} e^{-k_{10}x} f_{10}(y) + \sum_{n=0}^{\infty} a_n^S e^{k_{1n}(x+a)} f_{1n}(y) \right\}, \\ \phi_D^{S(2)} &= -\frac{ig}{\omega} \sum_{n=0}^{\infty} b_n^S \cosh k_{2n} x f_{2n}(y), \\ \phi_D^{S(3)} &= -\frac{ig}{\omega} \left\{ c_0^S f_{30}(y) + \sum_{n=1}^{\infty} c_n^S \cosh k_{3n} x f_{3n}(y) \right\},\end{aligned}\quad (15)$$

where $k_{10} = -ik_1, k_{20} = -ik_2$.

The eigenfunctions $f_{1n}(y), f_{2n}(y)$, and $f_{3n}(y)$ are given by

$$f_{1n}(y) = \begin{cases} \frac{\cosh k_1(y+h)}{\cosh k_1 h} & n=0, \\ \frac{\cos k_{1n}(y+h)}{\cos k_{1n} h} & n \geq 1. \end{cases} \quad (16)$$

$$f_{2n}(y) = \begin{cases} \frac{\cosh k_2(y+d)}{\cosh k_2 d} & n=0, \\ \frac{\cos k_{2n}(y+d)}{\cos k_{2n} d} & n \geq 1. \end{cases} \quad (17)$$

$$f_{3n}(y) = \frac{\cos k_{3n}(y+h)}{\cos k_{3n}(h-d)} \quad n \geq 0. \quad (18)$$

The eigenvalues k_{1n}, k_{2n}, k_{3n} are the solutions of the following equations

$$\begin{cases} k_1 \tanh k_1 h = \frac{\omega^2}{g}, k_{10} = -ik_1 & n=0, \\ k_{1n} \tan k_{1n} h = -\frac{\omega^2}{g} & n \geq 1. \end{cases} \quad (19)$$

$$\begin{cases} k_2 \tanh k_2 d = \frac{\omega^2}{g}, k_{20} = -ik_2 & n=0, \\ k_{2n} \tan k_{2n} d = -\frac{\omega^2}{g} & n \geq 1. \end{cases} \quad (20)$$

$$k_{3n} = \frac{n\pi}{(h-d)} \quad n \geq 0. \quad (21)$$

The unknown coefficients $a_n^S, b_n^S, c_n^S (n=0,1,2,\dots)$ can then be determined by invoking the continuity of potential and horizontal velocity at $x=-a$. The continuity of ϕ_D^S at $x=-a$ requires that

$$\begin{aligned} & \frac{1}{2} e^{k_{10}a} f_{10}(y) + \sum_{n=0}^{\infty} a_n^S f_{1n}(y) \\ &= \begin{cases} \sum_{n=0}^{\infty} b_n^S \cosh k_{2n} a f_{2n}(y) & -d \leq y \leq 0 \\ c_0^S f_{30}(y) + \sum_{n=1}^{\infty} c_n^S \cosh k_{3n} a f_{3n}(y) & -h \leq y \leq -d. \end{cases} \quad (22a,b) \end{aligned}$$

Multiplying (22a) by $f_{2m}(y)$ and integrating with respect to y over $[-d,0]$, we obtain

$$b_m^S \cosh k_{2m} a N_m^{(2)} = \frac{1}{2} e^{k_{10}a} C_{m0} + \sum_{n=0}^{\infty} a_n^S C_{mn}, \quad (23a)$$

where

$$\begin{aligned} C_{mn} &= \int_{-d}^0 f_{1n}(y) f_{2m}(y) dy, \\ \int_{-d}^0 f_{2n}(y) f_{2m}(y) dy &= \begin{cases} N_m^{(2)} & m=n \\ 0 & m \neq n. \end{cases} \end{aligned} \quad (23b)$$

If we multiply (22b) by $f_{3m}(y)$ and integrate with respect to y from $-h$ to $-d$, the following equation can be obtained.

$$\begin{aligned} m=0 \quad c_0^S N_0^{(3)} &= \frac{1}{2} e^{k_{10}a} D_{00} + \sum_{n=0}^{\infty} a_n^S D_{0n}, \\ m \neq 0 \quad c_m^S \cosh k_{3m} a N_m^{(3)} &= \frac{1}{2} e^{k_{10}a} D_{m0} + \sum_{n=0}^{\infty} a_n^S D_{mn}. \end{aligned} \quad (24a)$$

where

$$\begin{aligned} D_{mn} &= \int_{-h}^{-d} f_{1n}(y) f_{3m}(y) dy, \\ \int_{-h}^{-d} f_{3n}(y) f_{3m}(y) dy &= \begin{cases} N_m^{(3)} & m=n \\ 0 & m \neq n. \end{cases} \end{aligned} \quad (24b)$$

On the other hand, the continuity of $\frac{\partial \phi_D}{\partial x}$ at $x=-a$ gives

$$\begin{aligned} & -\frac{1}{2} k_{10} e^{k_{10}a} f_{10}(y) + \sum_{n=0}^{\infty} k_{1n} a_n^S f_{1n}(y) \\ &= \begin{cases} -\sum_{n=0}^{\infty} k_{2n} b_n^S \sinh k_{2n} a f_{2n}(y) & -d \leq y \leq 0 \\ -\sum_{n=1}^{\infty} k_{3n} c_n^S \sinh k_{3n} a f_{3n}(y) & -h \leq y \leq -d. \end{cases} \end{aligned} \quad (25)$$

Multiplying both sides of equation (25) by $f_{1m}(y)$ and integrating with respect to y from $-h$ to 0 , we obtain

$$\begin{aligned} m=0: & \\ & -\frac{1}{2} k_{10} e^{k_{10}a} N_0^{(1)} + k_{10} a_0^S N_0^{(1)} \\ &= -\sum_{n=0}^{\infty} k_{2n} b_n^S \sinh k_{2n} a C_{n0} - \sum_{n=1}^{\infty} k_{3n} c_n^S \sinh k_{3n} a D_{n0}, \\ m \neq 0: & \\ & k_{1m} a_m^S N_m^{(1)} \\ &= -\sum_{n=0}^{\infty} k_{2n} b_n^S \sinh k_{2n} a C_{nm} - \sum_{n=1}^{\infty} k_{3n} c_n^S \sinh k_{3n} a D_{nm}, \end{aligned} \quad (26)$$

where

$$\int_{-h}^0 f_{1n}(y) f_{1m}(y) dy = \begin{cases} N_m^{(1)} & m=n \\ 0 & m \neq n. \end{cases}$$

The final matrix equation for a_m^S can then be obtained by substituting equations (23) and (24) into equation (26):

$$\begin{aligned} a_0^S + \sum_{k=0}^{\infty} \frac{F_{0k}^S}{k_{10} N_0^{(1)}} a_k^S &= -\frac{1}{2} e^{k_{10}a} \left(\frac{F_{00}^S}{k_{10} N_0^{(1)}} - 1 \right) \quad m=0, \\ a_m^S + \sum_{k=0}^{\infty} \frac{F_{mk}^S}{k_{1m} N_m^{(1)}} a_k^S &= -\frac{1}{2} e^{k_{10}a} \frac{F_{m0}^S}{k_{1m} N_m^{(1)}} \quad m=1,2,3. \end{aligned} \quad (27a)$$

where

$$F_{mk}^S = \sum_{n=0}^{\infty} \frac{k_{2n} \tanh k_{2n} a C_{nm} C_{nk}}{N_n^{(2)}} + \sum_{n=1}^{\infty} \frac{k_{3n} \tanh k_{3n} a D_{nm} D_{nk}}{N_n^{(3)}}. \quad (27b)$$

By solving the above simultaneous algebraic equations, the unknown constants a_n^S can be determined. Subsequently, the other unknown constants b_n^S, c_n^S can be derived from equations (22) and (23) as follows:

$$b_n^S = \frac{\left(\frac{1}{2} e^{k_{10}a} C_{n0} + \sum_{k=0}^{\infty} a_k^S C_{nk} \right)}{\cosh k_{2n} a N_n^{(2)}} \quad n \geq 0, \quad (28)$$

$$c_n^S = \begin{cases} \frac{\left(\frac{1}{2} e^{k_{10}a} D_{00} + \sum_{k=0}^{\infty} a_k^S D_{0k} \right)}{N_0^{(3)}} & n=0, \\ \frac{\left(\frac{1}{2} e^{k_{10}a} D_{n0} + \sum_{k=0}^{\infty} a_k^S D_{nk} \right)}{\cosh k_{3n} a N_n^{(3)}} & n \geq 1. \end{cases}$$

Similarly, the asymmetric diffraction potentials in the three fluid regions are written as

$$\begin{aligned}\phi_D^{A(1)} &= -\frac{ig}{\omega} \left\{ \frac{1}{2} e^{-k_{10}x} f_{10}(y) + \sum_{n=0}^{\infty} a_n^A e^{k_{1n}(x+a)} f_{1n}(y) \right\}, \\ \phi_D^{A(2)} &= -\frac{ig}{\omega} \sum_{n=0}^{\infty} b_n^A \sinh k_{2n}x f_{2n}(y), \\ \phi_D^{A(3)} &= -\frac{ig}{\omega} \left\{ c_0^A \left(\frac{x}{a}\right) f_{30}(y) + \sum_{n=1}^{\infty} c_n^A \sinh k_{3n}x f_{3n}(y) \right\}.\end{aligned}\quad (29)$$

The unknown coefficients a_n^A, b_n^A, c_n^A can be determined in a similar manner by applying the continuity of potentials and horizontal velocities on $x = -a$:

$$\begin{aligned}a_0^A + \sum_{k=0}^{\infty} \frac{F_{0k}^A}{k_{10} N_0^{(1)}} a_k^A &= -\frac{1}{2} e^{k_{10}a} \left(\frac{F_{00}^A}{k_{10} N_0^{(1)}} - 1 \right) \quad m=0, \\ a_m^A + \sum_{k=0}^{\infty} \frac{F_{mk}^A}{k_{1m} N_m^{(1)}} a_k^A &= -\frac{1}{2} e^{k_{10}a} \frac{F_{m0}^A}{k_{1m} N_m^{(1)}} \quad m=1,2,3,\dots\end{aligned}\quad (30a)$$

where

$$\begin{aligned}F_{mk}^A &= \sum_{n=0}^{\infty} \frac{k_{2n} \coth k_{2n}a C_{nm} C_{nk}}{N_n^{(2)}} + \frac{D_{0m} D_{0k}}{aN_0^{(3)}} \\ &+ \sum_{n=1}^{\infty} \frac{k_{3n} \coth k_{3n}a D_{nm} D_{nk}}{N_n^{(3)}}.\end{aligned}\quad (30b)$$

The remaining unknown coefficients b_n^A and c_n^A can then be determined from:

$$\begin{aligned}b_n^A &= -\frac{\left(\frac{1}{2} e^{k_{10}a} C_{n0} + \sum_{k=0}^{\infty} a_k^A C_{nk}\right)}{\sinh k_{2n}a N_n^{(2)}} \quad n \geq 0, \\ c_n^A &= \begin{cases} \frac{\left(\frac{1}{2} e^{k_{10}a} D_{00} + \sum_{k=0}^{\infty} a_k^A D_{0k}\right)}{N_0^{(3)}} & n=0, \\ \frac{\left(\frac{1}{2} e^{k_{10}a} D_{n0} + \sum_{k=0}^{\infty} a_k^A D_{nk}\right)}{\sinh k_{3n}a N_n^{(3)}} & n \geq 1 \end{cases}\end{aligned}\quad (31)$$

2.2 Radiation Problem

The radiation potential of each mode, ϕ_{IR} , is governed by (2)-(5) and the following body-boundary condition:

$$\frac{\partial \phi_{IR}}{\partial y} = -i\omega f_1(x) \text{ on } y = -d - a \leq x \leq a. \quad (32)$$

For simplicity, we split ϕ_{IR} into symmetric and asymmetric parts as in the diffraction problem:

$$\phi_{IR}(x, y) = \phi_{IR}^S(x, y) + \phi_{IR}^A(x, y). \quad (33)$$

The radiation potentials in regions (II) and (III) can be represented by the sum of homogeneous solution and particular solution. The homogeneous solutions look similar to those considered in the diffraction problem. The symmetric radiation potentials in each region can be written as

$$\begin{aligned}\phi_{IR}^{S(1)} &= -\frac{ig}{\omega} \sum_{n=0}^{\infty} a_{1n}^S e^{k_{1n}(x+a)} f_{1n}(y), \\ \phi_{IR}^{S(2)} &= -\frac{ig}{\omega} \left\{ \sum_{n=0}^{\infty} b_{1n}^S \cosh k_{2n}x f_{2n}(y) + \frac{i\omega}{g} \tilde{\phi}_{IR}^{S(2)}(x, y) \right\}, \\ \phi_{IR}^{S(3)} &= -\frac{ig}{\omega} \left\{ c_{10}^S f_{30}(y) + \sum_{n=1}^{\infty} c_{1n}^S \cosh k_{3n}x f_{3n}(y) \right. \\ &\quad \left. + \frac{i\omega}{g} \tilde{\phi}_{IR}^{S(3)}(x, y) \right\}.\end{aligned}\quad (34)$$

The asymmetric radiation potentials can be expressed in a similar manner:

$$\begin{aligned}\phi_{IR}^{A(1)} &= -\frac{ig}{\omega} \sum_{n=0}^{\infty} a_n^A e^{k_{1n}(x+a)} f_{1n}(y), \\ \phi_{IR}^{A(2)} &= -\frac{ig}{\omega} \left\{ \sum_{n=0}^{\infty} b_{1n}^A \sinh k_{2n}x f_{2n}(y) + \frac{i\omega}{g} \tilde{\phi}_{IR}^{A(2)}(x, y) \right\}, \\ \phi_{IR}^{A(3)} &= -\frac{ig}{\omega} \left\{ c_{10}^A \left(\frac{x}{a}\right) f_{30}(y) + \sum_{n=1}^{\infty} c_{1n}^A \sinh k_{3n}x f_{3n}(y) \right. \\ &\quad \left. + \frac{i\omega}{g} \tilde{\phi}_{IR}^{A(3)}(x, y) \right\}.\end{aligned}\quad (35)$$

The particular solutions in (II) and (III) satisfying the inhomogeneous body-boundary condition can be obtained as

$$\tilde{\phi}_{IR}^{S(2)} = \frac{-i\omega \cos(m_1 x)(m_1 \cosh m_1 y + \nu \sinh m_1 y)}{m_1(-m_1 \sinh m_1 d + \nu \cosh m_1 d)}. \quad (36)$$

$$\tilde{\phi}_{IR}^{A(2)} = \frac{-i\omega \sin(m_2 x)(m_2 \cosh m_2 y + \nu \sinh m_2 y)}{m_2(-m_2 \sinh m_2 d + \nu \cosh m_2 d)}. \quad (37)$$

$$\tilde{\phi}_{IR}^{S(3)} = \frac{-i\omega \cos(m_1 x) \cosh m_1 (y+h)}{m_1 \sinh m_1 (h-d)} \quad (38)$$

$$\tilde{\phi}_{IR}^{A(3)} = \frac{-i\omega \sin(m_2 x) \cosh m_2 (y+h)}{m_2 \sinh m_2 (h-d)} \quad (39)$$

where

$$m_1 = (\lambda_1^S / a), \quad m_2 = (\lambda_1^A / a).$$

The unknown constants in equations (34) and (35) can be determined in a similar manner to the diffraction problem using the matching conditions at $x = -a$. The simultaneous algebraic equations for the unknown constants $a_{ik}^{S,A}$ in region (I) are given by

$$a_{lm}^{S,A} + \sum_{k=0}^{\infty} \frac{F_{mk}^{S,A}}{k_{1m} N_m^{(1)}} a_{ik}^{S,A} = \frac{X_{ml}^{S,A}}{k_{1m} N_m^{(1)}} \quad (m=0,1,2,3,\dots), \quad (40)$$

where

$$X_{ml}^{S,A} = \frac{i\omega}{g} \left\{ \int_{-d}^0 \frac{\partial \tilde{\phi}_{IR}^{S,A(2)}(-a,y)}{\partial x} f_{lm}(y) dy \right. \\ \left. + \int_{-h}^{-d} \frac{\partial \tilde{\phi}_{IR}^{S,A(3)}(-a,y)}{\partial x} f_{lm}(y) dy \right\}. \quad (41)$$

The other unknown coefficients can be determined from

$$b_{in}^S = - \frac{\left\{ \frac{i\omega}{g} \int_{-d}^0 \tilde{\phi}_{IR}^{S(2)} f_{2n}(y) dy - \sum_{k=0}^{\infty} a_{ik}^S C_{nk} \right\}}{\cosh k_{2n} a N_n^{(2)}} \quad n \geq 0,$$

$$c_{in}^S = \begin{cases} \frac{\left\{ \frac{i\omega}{g} \int_{-h}^{-d} \tilde{\phi}_{IR}^{S(3)} f_{30}(y) dy - \sum_{k=0}^{\infty} a_{ik}^S D_{0k} \right\}}{N_0^{(3)}} & n=0 \\ \frac{\left\{ \frac{i\omega}{g} \int_{-h}^{-d} \tilde{\phi}_{IR}^{S(3)} f_{3n}(y) dy - \sum_{k=0}^{\infty} a_{ik}^S D_{nk} \right\}}{\cosh k_{3n} a N_n^{(3)}} & n \geq 1 \end{cases} \quad (42a)$$

and

$$b_{in}^A = \frac{\left\{ \frac{i\omega}{g} \int_{-d}^0 \tilde{\phi}_{IR}^{A(2)} f_{2n}(y) dy - \sum_{k=0}^{\infty} a_{ik}^A C_{nk} \right\}}{\sinh k_{2n} a N_n^{(2)}} \quad n \geq 0,$$

$$c_{in}^A = \begin{cases} \frac{\left\{ \frac{i\omega}{g} \int_{-h}^{-d} \tilde{\phi}_{IR}^{A(3)} f_{30}(y) dy - \sum_{k=0}^{\infty} a_{ik}^A D_{0k} \right\}}{N_0^{(3)}} & n=0 \\ \frac{\left\{ \frac{i\omega}{g} \int_{-h}^{-d} \tilde{\phi}_{IR}^{A(3)} f_{3n}(y) dy - \sum_{k=0}^{\infty} a_{ik}^A D_{nk} \right\}}{\sinh k_{3n} a N_n^{(3)}} & n \geq 1 \end{cases} \quad (42b)$$

2.3 Membrane Response

Neglecting viscous (or material) damping, the motion of membrane is governed by the inhomogeneous one-dimensional wave equation as follows:

$$T \frac{d^2 \xi}{dx^2} + m\omega^2 \xi = -i\rho\omega[\phi^{(3)}(x,-d) - \phi^{(2)}(x,-d)], \quad (43)$$

where T , ρ , and m are the membrane tension, fluid density, and membrane mass per unit length, respectively.

Substituting

$$\phi(x,y) = \phi_D(x,y) + \sum_{j=1}^{\infty} \zeta_j \phi_{jR}(x,y) \quad \xi(x) = \sum_{j=1}^{\infty} \zeta_j f_j(x)$$

into (43) yields

$$\sum_{j=1}^{\infty} \zeta_j \left\{ -T \frac{d^2 f_j(x)}{dx^2} - m\omega^2 f_j(x) - p_{jR}(x) \right\} = p_D(x), \quad (44a)$$

where

$$p_{jR}(x) = i\rho\omega[\phi_{jR}^{(3)}(x,-d) - \phi_{jR}^{(2)}(x,-d)], \\ p_D(x) = i\rho\omega[\phi_D^{(3)}(x,-d) - \phi_D^{(2)}(x,-d)]. \quad (44b)$$

Multiplying the above equation by $f_i(x)$ and integrating over the membrane, we obtain

$$\sum_{j=1}^{\infty} \{ K_{ij} - \omega^2 (M_{ij} + a_{ij}) - i\omega b_{ij} \} \zeta_j = F_i \quad i=1,2,3,\dots, \quad (45a)$$

where

$$\begin{aligned}
 K_y &= -\int_{-a}^a T \frac{d^2 f_j(x)}{dx^2} f_i(x) dx, \\
 M_y &= \int_{-a}^a m f_j(x) f_i(x) dx, \\
 a_y &= \Re\left\{\frac{1}{\omega^2} \int_{-a}^a p_{jR}(x) f_i(x) dx\right\}, \\
 b_y &= \Im\left\{\frac{1}{\omega} \int_{-a}^a p_{jR}(x) f_i(x) dx\right\}, \\
 F_i &= \int_{-a}^a p_D(x) f_i(x) dx.
 \end{aligned} \tag{45b}$$

The symbols $K_y, M_y,$ and F_i represent the generalized (modal) stiffness matrix, mass matrix and force vector, respectively, and a_y and b_y are the generalized added-mass and radiation-damping matrix. Truncating the series of (45a) at the appropriate term M , we can solve for the unknown complex amplitudes ζ_j corresponding to each mode. When the membrane is on the free surface, a hydrostatic correction term needs to be added.

Finally, the reflection and transmission coefficients can be determined from

$$\begin{aligned}
 R_f &= |(a_0^S + a_0^A) + \sum_{i=1}^{\infty} \zeta_i (a_{iR}^S + a_{iR}^A)| e^{k_{i0}a}, \\
 T_f &= |(a_0^S - a_0^A) + \sum_{i=1}^{\infty} \zeta_i (a_{iR}^S - a_{iR}^A)| e^{k_{i0}a}.
 \end{aligned} \tag{46}$$

The vertical hydrodynamic forces on the horizontal membrane can be calculated from

$$F = -i\rho\omega \int_{-a}^a [\phi^{(3)}(x,-d) - \phi^{(2)}(x,-d)] dx. \tag{47}$$

3. Experiments

In order to validate the theory and numerical procedure developed in the preceding section, we conducted a series of experiments in the two-dimensional wave tank (37 m long, 0.91 m wide, and 1.22 m deep) located at Texas A&M University. The glass-walled wave tank

is equipped with a dry-back, hinged flap wave maker capable of producing regular and irregular waves.

The wave elevation was measured with a resistance wave gauge having an accuracy of ± 0.1 cm. A probe measuring incident and reflected wave heights and another probe measuring the transmitted wave heights are placed at 9.1 m and 22.9m from the wavemaker, respectively. The wave barrier model was placed at 18.3m from the wavemaker between the two probes. Regular waves were generated by a user-defined time-voltage input to the wave maker. The wave frequency range used in our experiments was from 0.5 to 1.4Hz. The wave heights used in our experiments are 6cm, 8cm and 10cm, respectively. The time series of the generated regular wave packet was sinusoidal with the beginning and end of the series attenuated in amplitude.

The model membrane ($m = 0.17 \text{ kg/m}^2$) was made of a thin plastic material resembling a plastic tarpaulin. The length and width of the membrane were 80cm and 82cm, respectively. The ends of the membrane were attached to two horizontal steel bars which are fixed by four vertical steel frames clamped to the tank, as shown in Fig.1b.

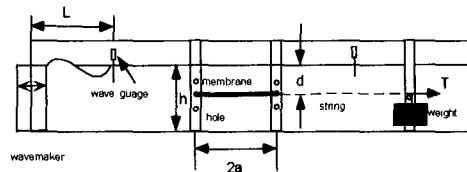


Fig. 1b Experimental set-up of a submerged horizontal membrane breakwater

The tension on the membrane was provided by a series of string-weight units. The end-bar of the tensioned membrane was then

fixed to a new location of the steel frame. After a tension is correctly given, the string-weight units were removed. Table 1 summarizes the principal characteristics of the models used in our experiments.

Table 1 Experimental conditions

	Exp.#1	Exp.#2
Membr. Length	80cm	80cm
Membr. Width	82cm	82cm
Subm. Depth	16cm	0
Water Depth	80cm	56cm
Membr. Tension	21kgF	36kgF
Wave Frequency	0.5-1.4Hz	0.5-1.4Hz
Wave Amplitude	3cm	3cm

The signal of the incident wave train was obtained as it passes the probe toward the membrane breakwater. Then, the reflected wave train was recorded as the reflected waves pass the probe again in the opposite direction. After averaging the wave heights for the incident and reflected, and transmitted wave trains, the reflection coefficient R_r and transmission coefficient T can be calculated from the ratio of the averaged reflected and transmitted wave height to the averaged incident wave height. We observed that reflected and transmitted waves were repeatedly reflected from the wave maker and beach as the time goes on. In order to minimize the effects of multiple reflection, the present method was adopted in favor of moving single probe method or three-probe method [Isaacson, 1991], which require relatively longer time to establish a steady state. It is shown in Hagen [1994] that the present method is more reliable than the moving-probe or three-probe methods when nonlinear phenomena or multiple reflections exist. In most of our surface-piercing-buoy experiments, the errors estimated from the energy relation were able to be kept within

10%. The discrepancy can be attributed to viscous, gap, and nonlinear effects, and membrane material damping etc. When the membrane is located on or very close to the calm water level, the energy-conservation error is increased due to wave overtopping over the membrane.

4. Numerical Results and Discussions

The analytic solutions for impermeable membrane are developed as described in Sec. 2. First, the convergence of analytic solutions with the number of natural modes M is shown in Fig.2. It is seen that the convergence with those parameters is rapid. In the following, the analytic solutions with $M=5, N=10$ were used to investigate the performance of a horizontal flexible membrane wave barrier for various design conditions. The membrane mass per unit length used for these numerical examples was 1kg/m.

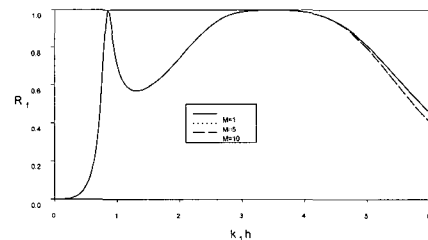


Fig. 2 Convergence of reflection coefficient with the number of natural modes of membrane for the case $d/h=0.2, a/h=0.5, T/\rho gh^2=0.1$ and $N=10$ (N =number of eigenfunctions)

In Figures 3a and 3b, the transmission coefficients and hydrodynamic loading on a particular membrane are plotted for various membrane tensions. It is seen that there exists an optimal tension for the given design condition. The infinite-tension case corresponds to the diffraction by a rigid

horizontal plate which was also studied by McIver[1985] for the normal incidence case. The correctness of the limiting case was also checked against McIvers results. In Fig.5b, the hydrodynamic loading for the lower tension (or more flexible membrane) tends to be smaller but has a larger peak near the resonance region.

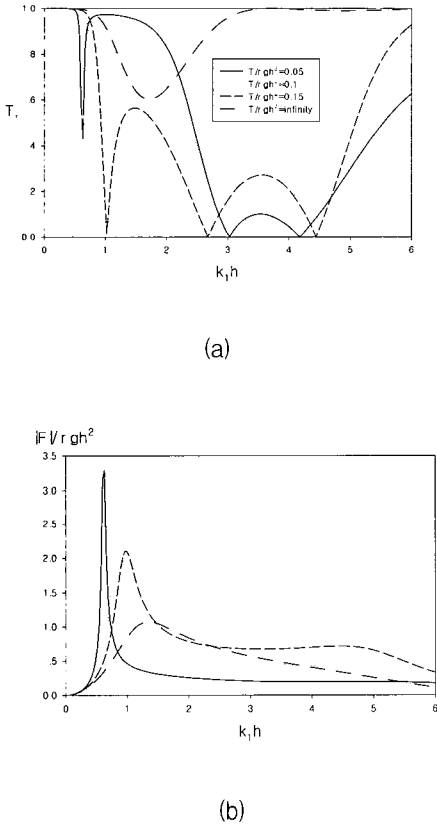


Fig. 3 Transmission coefficient (a) and hydrodynamic loading (b) of a submerged horizontal membrane breakwater as function of non-dimensional tension $T/\rho gh^2$ and wavenumber $k_1 h$ for $d/h = 0.2, a/h = 0.5$

In Figure 4, the membrane tension and width are fixed and the submergence depth is varied from 0 to $0.3h$. For this example, the overall efficiency is best for the case

$d=0.2h$. The trend of the limiting case $d=0$ (membrane on the calm water surface) is quite different from that of the other curves because only the lower part of the surface-mounted membrane is exposed to the fluid loading. In Fig. 5, the amplitudes of membrane responses are plotted for the cases $d=0.1h$ and $0.2h$ as function of dimensionless x coordinate and

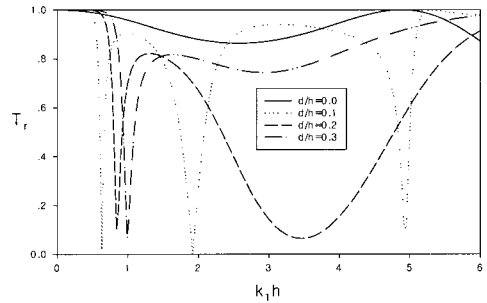


Fig. 4 Transmission coefficients of a submerged impermeable membrane breakwater as function of submergence depth d/h and function of wavenumber $k_1 h$ for $a/h = 0.5, T/\rho gh^2 = 0.1$

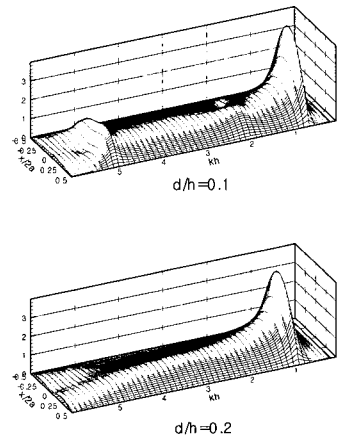


Fig. 5 Responses of a membrane ($|\xi|/A$) as function of wavenumber $k_1 h$ and horizontal coordinate $x/2a$ for $d/h = 0.1, 0.2, a/h = 0.5, T/\rho gh^2 = 0.1$

wavenumbers. It is interesting to see that the performance is still good near $k_1 h = 1$ despite large sinusoidal membrane motions. The motion amplitudes are much smaller than the incident wave amplitude except for the resonance region.

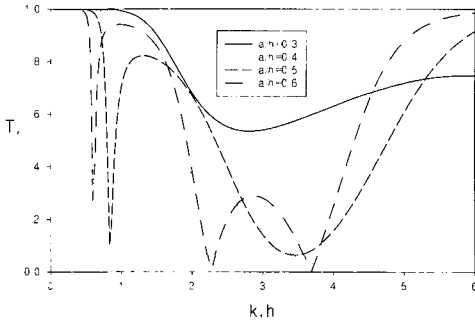


Fig.6 Transmission coefficients of a submerged impermeable membrane breakwater as function of length of membrane a/h and wavenumber $k_1 h$ for $d/h = 0.2, T/\rho g h^2 = 0.1$

In the next figure (Fig.6), the membrane tension and submergence depth are fixed and the size (width) of membrane is varied from $a = 0.3h$ to $0.6h$. Interestingly, the bandwidth of the high performance region is largest when $a = 0.4h$, which implies that the efficiency is not necessarily improved with the size of membrane.

Finally, the computational results for impermeable membrane are compared with the experimental results conducted in the 2D wave tank located at Texas A&M University. The measured values generally follow the trend of computed curves. The same experiment was conducted for three different incident wave amplitudes, and the general trend looks similar. It can be seen in Fig.7 that the wave blocking performance is indeed good in the range $0.8 < f < 1.3$ (Hz), as predicted by the present linear hydro-elastic theory. We can

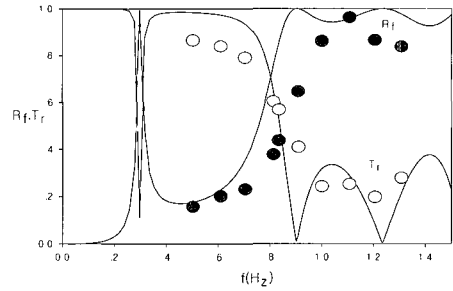


Fig. 7 Comparison of analytic results with measured values (Exp.1) for a submerged horizontal membrane breakwater ; analytic solution (—), experimental results R_1 (dark) and T_1 (white)

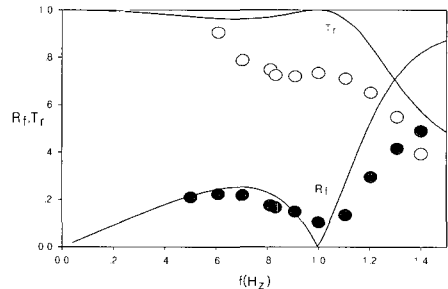


Fig. 8 Comparison of analytic results with measured values (Exp.2) for a floating horizontal membrane breakwater ; analytic solution (—), experimental results R_1 (dark) and T_1 (white)

notice that its effect is the largest near the resonance region ($f \approx 0.35$ Hz). The discrepancy between predicted and measured results can be attributed to the uncertainties pertaining to the amount of viscous (or material) damping, nonlinear effects, gap or end effects etc. In particular, we observed during the experiment that the membrane response was not perfectly uniform in the y direction. The next figure

(Fig.8) shows similar comparisons for the surface-mounted membrane. The performance of this particular design is not good unless $f > 1.2\text{Hz}$. For this particular case, the wave over-topping over the surface-mounted membrane adds more uncertainty with regard to the validity of the present theoretical model. Despite the additional uncertainty, the trend of experimental values follows reasonably that of predicted values.

5. Summary and Conclusions

The interaction of monochromatic incident waves with a horizontal flexible membrane was investigated in the context of two-dimensional linear hydro-elastic theory. In Sec.2, analytic diffraction and radiation solutions for a submerged impermeable horizontal membrane were obtained by matching the eigenfunction solutions in the three fluid domains. The linear hydro-elastic theory was then compared with a series of experiments conducted with an impermeable membrane and a reasonable agreement was obtained.

Using the developed computer program, the performance of surface-mounted or submerged impermeable horizontal membrane wave barriers was tested with various membrane tensions, widths, and submergence depths. It was seen that an optimal combination of design parameters existed for given water depths and wave characteristics. From the present study, it can be concluded that a properly designed horizontal flexible membrane can be a very effective wave barrier and its optimal design can be found through a comprehensive parametric study using the developed theory and computer programs. To further verify its practicality, a more rigorous nonlinear time-domain numerical analysis and larger-scale experiments need to be done.

Acknowledgment

This research was sponsored by the Ministry of Trade, Industry and Energy (MOTIE) through a KRISO/TAMU cooperative research program. This work was also partly supported by the Samgong Industrial Co.,Ltd.

References

- [1] Abul-Azm, A.G., 1994, Wave diffraction by double flexible breakwaters, *Journal of Applied Ocean Research*, Vol.16, 87-99.
- [2] Aoki, S., Liu, H., & Sawaragi, T., 1994, Wave transformation and wave forces on submerged vertical membrane, *Proc. Intl. Symp. Waves - Physical and Numerical Modeling*, Vancouver, 1287-1296
- [3] Dean, R.G. & Dalrymple, R.A., 1984, *Water Wave Mechanics for Engineers and Scientists*, World Scientific Publishing Co.
- [4] Isaacson, M., 1991, Measurement of regular wave, *ASCE J. of Waterway, Port, Coastal & Ocean Engineering*, Vol.117, 553-569
- [5] Kee, S.T. & Kim, M.H., 1997, Flexible membrane wave barrier. Part 2. Floating/submerged buoy-membrane system, *ASCE J. of Waterway, Port, Coastal & Ocean Engineering*, Vol.123, No.2, 82-90.
- [6] Kim, M.H. & Kee, S.T., 1996, Flexible membrane wave barrier. Part 1. Analytic and numerical solutions, *ASCE J. of Waterway, Port, Coastal & Ocean Engineering*, Vol.122, No.1, 46-53.
- [7] Lee, J.F. & Chen, C.J., 1990, Wave interaction with hinged flexible breakwater, *J. of Hydraulic Research*, Vol 28, 283-295.
- [8] McIver, M., 1985, Diffraction of water waves by a moored, horizontal, flat plate, *J. of Engineering Mathematics*, Vol 19, No.4, 297-320.
- [9] Newman, J.N., 1994, Wave effects on

The Performance of a Horizontal Flexible Membrane Breakwater in Waves

deformable bodies, J. of Applied Ocean Research, Vol.16, 47-59.

[10] Siew, P.F. & Hurley, D.G., 1977, Long surface waves incident on a submerged horizontal plate, J. of Fluid Mechanics, Vol.83, 141-151

[11] Thompson, G.O., Sollitt, C.K., McDougal, W.G. & Bender W.R., 1992, Flexible membrane wave barrier, ASCE Conf. Ocean V, College Station, 129-148.

[12] Williams, A.N., Geiger, P.T., & McDougal, W.G., 1991, Flexible floating breakwater, ASCE J. of Waterway, Port, Coastal & Ocean Engineering, Vol 117, #5, 429-450.

[13] Williams, A.N., 1996, Floating membrane breakwater, J. of Offshore Mechanics & Arctic Engr., Vol 118, 46-51.